An improved model-free predictive voltage control for grid-forming inverter with adaptive ultra-local data-model in renewable energy system

Yifu Lin[1]*, Junwei Zhu[2] and Feng He[2]

[1]Country State Grid Fujian Electric Power Co., Ltd., Fuzhou, China, [2]Putian Electric Power Supply Company of State Grid Fujian Electric Power Co., Ltd., Putian, China

Conventional model-based predictive voltage control (MBPVC) for grid-forming inverters (GFIs) in renewable energy system is sensitive to parametric accuracy. To address this issue, an improved model-free predictive voltage control (MFPVC) is proposed for grid-forming inverter. First, the parametric impact on MBPVC is analyzed in GFI. Then, the adaptive ultra-local data-model (ULDM) of the GFI is established for model-free voltage prediction. The ULDM of GFI is updated in each control period by combining the capacitor voltage gradient relationship. The linear extended-state-observer with the adaptive strengthening factor is designed to enhance the performance of the ULDM. Additionally, the optimal switching sequence is proposed for further reducing voltage ripples. The duration of each voltage vector in corresponding optimal switching sequence is calculated based on the deadbeat principle. The proposed MFPVC method effectively eliminates parametric effect and improve the accuracy of model-free voltage prediction. Finally, the conventional MBPVC, conventional MFPVC and proposed MFPVC are compared by the designed hardware experimental platform of GFI.

KEYWORDS

grid-forming inverter, model-free predictive voltage control, adaptive ultra-local data-model, optimal switching sequence, parameter robustness

1 Introduction

With the rapid development of renewable energy system, microgrids have been widely promoted and applied. They integrate renewable energy and distributed generation with traditional power systems, enhancing energy utilization and microgrid system reliability (Tan et al., 2024). In microgrid systems, renewable energy grid-forming inverters (GFIs) serve as key components, efficiently converting DC power to AC. By incorporating LC filters, they reduce output voltage harmonics, meeting the diverse needs of microgrid loads and providing reliable grid voltage (Song et al., 2022; Liu and Wang, 2022).

Model-based predictive voltage control (MBPVC) demonstrates excellent dynamic response and multi-objective optimization capabilities in voltage regulating

support of GFIs, making it highly effective in complex microgrids (Rui et al., 2024; Samanta et al., 2024; Liu and Wang, 2022). MBPVC uses the discrete mathematical model of the GFI to predict future system states and selects the optimal voltage vector based on a predefined cost function (Zheng et al., 2021). However, the performance of model-based voltage prediction in conventional MBPVC is highly dependent on the accuracy of inverter system parameters. Mismatched model parameters can degrade prediction accuracy, reducing voltage prediction accuracy and potentially harming the entire system (Yin et al., 2024a; Rui et al., 2023; Hu et al., 2023).

To enhance the parameter robustness of MBPVC, researchers have proposed various robust MBPVC methods for GFIs. These include disturbance observer-based MBPVC (Jin et al., 2022; Zhao et al., 2023; Zhang et al., 2021), and parameter identification-based MBPVC (Long et al., 2022a; Long et al., 2022b; Lian et al., 2023). Disturbance observer-based MBPVC uses various observers to estimate parameters and system disturbances, improving voltage prediction accuracy in MBPVC. Ref. (Jin et al., 2022). employs a sliding mode observer for robust grid voltage control. Ref. (Zhao et al., 2023). uses a Kalman filter for the same purpose. Ref. (Zhang et al., 2021). applies an extended state observer to observe and suppress system disturbances, enhancing voltage robustness. However, disturbance observer-based MBPVC requires real-time adjustment of observer gains under different conditions to ensure observation accuracy.

Additionally, researchers have proposed parameter identification-based MBPVC, utilizing voltage and current data from GFIs along with various algorithms to estimate system parameters and build accurate models. Ref. (Long et al., 2022a). presents a gradient descent optimization method for online calculation of inductor and capacitor. Ref. (Long et al., 2022b). introduces a moth-flame optimization parameter identification method. Ref. (Lian et al., 2023). employs recursive least squares for online identification of inverter system parameters, enhancing MBPVC's parameter robustness. However, the accuracy of parameter identification is susceptible to external disturbances, and identification errors can still impact voltage prediction for GFIs.

In recent years, researchers have proposed model-free predictive voltage control (MFPVC) to improve the robustness of voltage prediction in GFIs. These methods use system data and historical information to predict future states without relying on accurate mathematical models. In Ref. (Heydari et al., 2022), researchers used an autoregressive exogenous input model to replace traditional mathematical models, but this approach requires substantial system data and employs the least squares method for gain estimation, increasing computational burden. Refs. (Hu et al., 2024; Yin et al., 2024b). introduce the voltage-current gradient based MFPVC, but these methods necessitate designing gradient update techniques to ensure accuracy. Ref. (Su et al., 2024). presents the ultra-local data models based MFPVC, which is simple to implement but uses multiple cycles of voltage and current data, reducing response speed.

To address the aforementioned issues, this paper proposes an improved model-free predictive voltage control (MFPVC) method for GFI in renewable energy system. First, the parametric
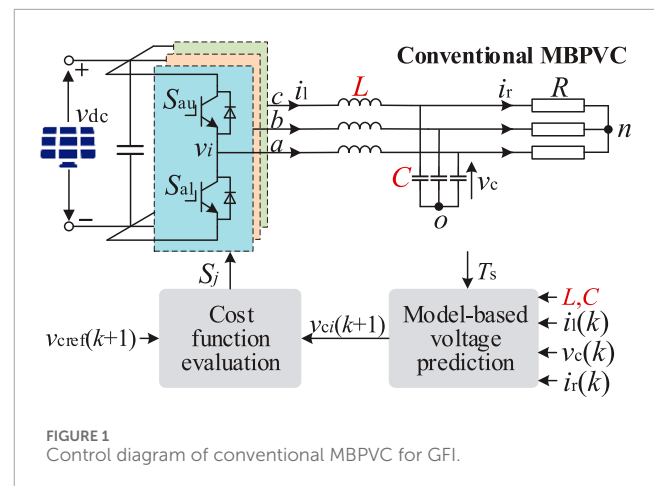

FIGURE 1
Control diagram of conventional MBPVC for GFI.

impact on traditional MBPVC in GFI is analyzed. Then, an improved MFPVC method is presented, which establishes and updates the ultra-local data-model (ULDM) of the GFI by using the capacitor voltage gradient relationship for model-free voltage prediction. The performance of proposed ULDM is enhanced by the linear extended-state-observer (LESO) with strengthening. Additionally, to further improve the accuracy of model-free voltage prediction, the optimal switching sequence is designed, and its corresponding duration is calculated based on the deadbeat principle. Finally, experimental results validate the effectiveness of the proposed MFPVC method. The mainly contributions of proposed MFPVC include: (1) it eliminates parametric effect in comparison with conventional MBPVC (Rui et al., 2024; Samanta et al., 2024; Liu and Wang, 2022; Zheng et al., 2021); (2) it avoids the use of multiple cycle data and improves dynamic performance in comparison with conventional MFPVC (Su et al., 2024).

2 Conventional MBPVC method for GFIs under parameter mismatch

As shown in Figure 1, conventional MBPVC is widely used in GFIs for capacitor voltage regulation (Zheng et al., 2021). The model-based voltage prediction obtains the future state of capacitor voltage for each basic voltage vector. The predicted capacitor voltage is then used in the cost function evaluation to assess the voltage error for each basic voltage vector. The vector with the smallest error is selected as the optimal voltage vector. Based on its corresponding three-phase switch state, the three-phase switch functions S_j are set to drive the upper half-bridge switches S_{ju} and lower half-bridge switches S_{jl} (j = a, b, c).

2.1 Model-based voltage prediction

Figure 1 shows the GFI under conventional MBPVC method, where L is the filter inductor, C is the filter capacitor and R is the resistance load. v_{dc} is the renewable energy DC source, v_i is the voltage vector (i = 0~7), v_c is the capacitor voltage, i_l is the inductor

current and i_r is the load current. The three-phase switch functions S_j can be expressed as

$$S_j = \begin{cases} 1, S_{j\text{u}} \text{ on } \& \ S_{j\text{l}} \text{ off} \\ 0, S_{j\text{u}} \text{ off } \& \ S_{j\text{l}} \text{ on} \end{cases}. \quad (1)$$

Based on Figure 1, the mathematical model of the GFI can be expressed as

$$\begin{cases} L\dfrac{di_{\text{l}}}{dt} = v_i - v_{\text{c}} \\ C\dfrac{dv_{\text{c}}}{dt} = i_{\text{l}} - i_{\text{r}} \end{cases}. \quad (2)$$

According to the forward Euler method, Equation 2 can be discretized as

$$\begin{cases} i_{\text{l}}(k+1) = i_{\text{l}}(k) + \dfrac{T_s}{L}\big(v_i(k+1) - v_{\text{c}}(k)\big) \\ v_{\text{c}}(k+1) = v_{\text{c}}(k) + \dfrac{T_s}{C}(i_{\text{l}}(k+1) - i_{\text{r}}(k)) \end{cases}. \quad (3)$$

Equation 3 can be further deduced as

$$v_{ci}(k+1) = v_{\text{c}}(k) + \frac{T_s^2}{LC}\big(v_i(k+1) - v_{\text{c}}(k)\big) + \frac{T_s}{C}(i_{\text{l}}(k) - i_{\text{r}}(k)). \quad (4)$$

According to Equation 4, by substituting different basic voltage vectors $v_i(k+1)$ and sampling $v_{\text{c}}(k)$, $i_{\text{l}}(k)$, $i_{\text{r}}(k)$, along with parameters L and C, the model-based capacitor voltage can be predicted.

2.2 Cost function evaluation

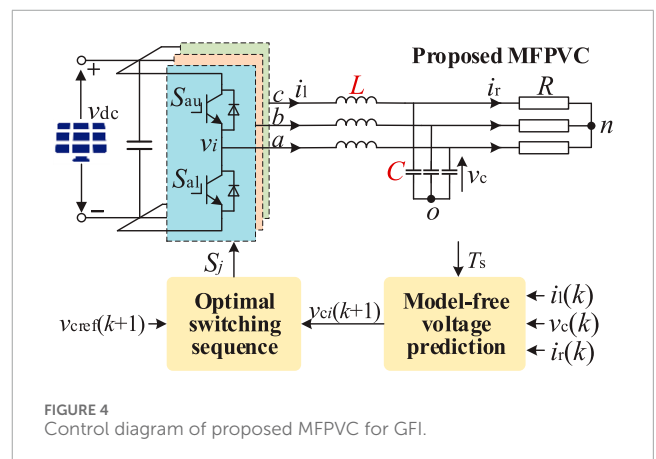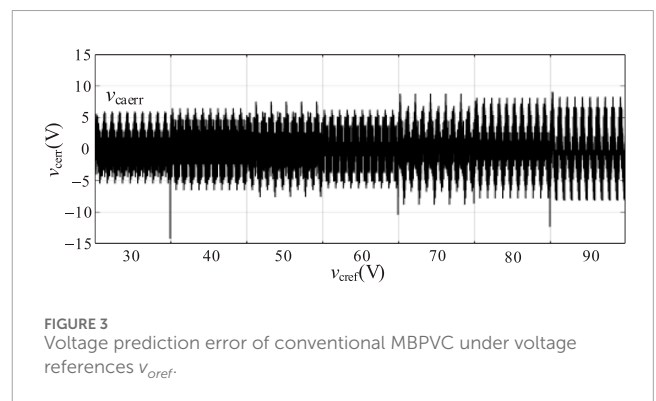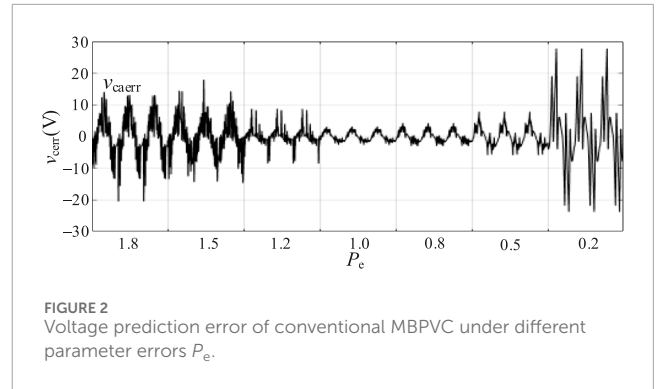To select the optimal voltage vector from basic voltage vectors v_0 to v_7, a cost function g is defined as

$$g = \big(v_{\text{cref}}(k+1) - v_{ci}(k+1)\big)^2. \quad (5)$$

where v_{cref} is the capacitor voltage reference. The optimal voltage vector obtained from Equation 5 enables the control of the three-phase switches $S_{j\text{u}}$ and $S_{j\text{l}}$.

2.3 Analysis of conventional MBPVC

According to Equation 4, the accuracy of model-based voltage prediction $v_{ci}(k+1)$ is influenced by the inductance L and capacitance C parameters. When the model parameters L_{m} and C_{m} do not match the actual parameters L and C, the prediction performance of $v_{ci}(k+1)$ would be affected. Figure 2 illustrates the prediction error v_{cerr} due to parameter mismatch, where the parameter error $P_{\text{e}} = L_{\text{m}}/L = C_{\text{m}}/C$. As seen in Figure 2, the prediction error v_{cerr} increases with the parameter error P_{e}.

In addition, based on Equation 4, the accuracy of model-based voltage prediction $v_{ci}(k+1)$ is also influenced by the basic voltage vector $v_i(k+1)$. Due to the limited number of basic voltage vectors $v_i(k+1)$ in GFIs, the prediction error v_{cerr} is also affected. Figure 3 illustrates the prediction error v_{cerr} due to the application of basic voltage vector $v_i(k+1)$, where different voltage references v_{cref} is set. As seen in Figure 3, the prediction error v_{cerr} consistently remains around 5 V.

FIGURE 2
Voltage prediction error of conventional MBPVC under different parameter errors P_e.

FIGURE 3
Voltage prediction error of conventional MBPVC under voltage references v_{oref}.

FIGURE 4
Control diagram of proposed MFPVC for GFI.

3 Proposed MFPVC method for GFIs

To mitigate the impact of parameter variations on the voltage prediction, a model-free predictive voltage control (MFPVC) method is proposed, as shown in Figure 4. This method is composed of model-free voltage prediction and optimal switching sequence. The former is utilized for eliminating parametric effect and the latter is utilized for reducing prediction errors.
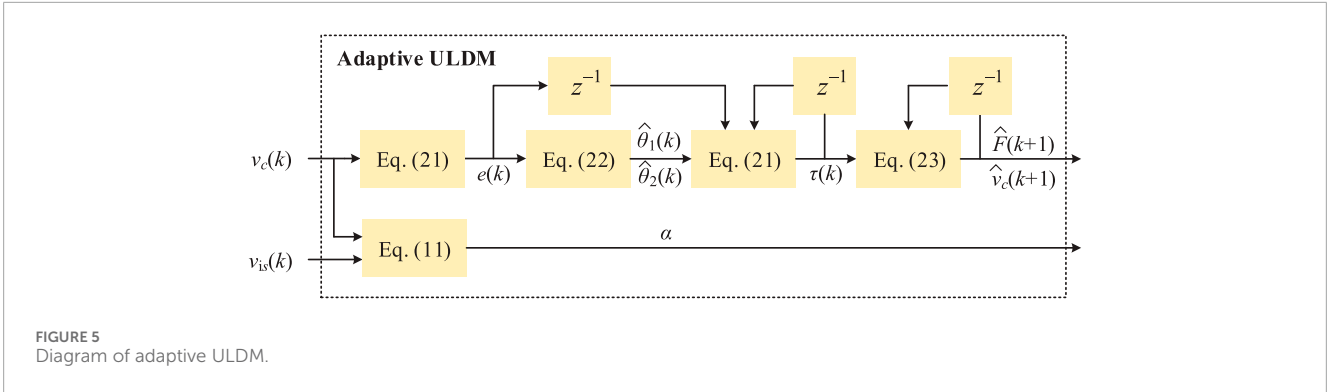
FIGURE 5
Diagram of adaptive ULDM.

TABLE 1 Optimal switching sequence.

Sector	Switching sequence
I	$v_0\ v_1\ v_2\ v_7\ v_7\ v_2\ v_1\ v_0$
II	$v_0\ v_3\ v_2\ v_7\ v_7\ v_2\ v_3\ v_0$
III	$v_0\ v_3\ v_4\ v_7\ v_7\ v_4\ v_3\ v_0$
IV	$v_0\ v_5\ v_4\ v_7\ v_7\ v_4\ v_5\ v_0$
V	$v_0\ v_5\ v_6\ v_7\ v_7\ v_6\ v_5\ v_0$
VI	$v_0\ v_1\ v_6\ v_7\ v_7\ v_6\ v_1\ v_0$

3.1 Proposed model-free voltage prediction

3.1.1 Development of ultra-local data-model

According to Equation 2, the ULDM of the GFI can be expressed as

$$\frac{dv_c}{dt} = \alpha U_i + F,\qquad(6)$$

where $\alpha = T_s/L/C$, $U_i = v_i - v_c$, $F = (i_l - i_r)/C + F_0$, F_0 are the gain, input, concentrated disturbance and nonlinear disturbance of the ULDM.

3.1.2 Updating of ultra-local data-model

Based on Equation 6, the capacitor voltage gradient g_{ci} can be obtained as

$$g_{ci}(k) = \frac{v_c(k) - v_c(k-1)}{T_s} = \alpha U_i(k-1) + F(k),\qquad(7)$$

Similarly, Equation 7 can be deduced as

$$g_{ci}(k-1) = \frac{v_c(k-1) - v_c(k-2)}{T_s} = \alpha U_i(k-2) + F(k-1).\qquad(8)$$

Subtracting Equation 8 from Equation 7 yields that

$$g_{ci}(k) - g_{ci}(k-1) = \alpha\big(U_i(k-1) - U_i(k-2)\big) + (F(k) - F(k-1)).\qquad(9)$$

Since the GFI usually operates at a high sampling and control frequency, it can be assumed that $F(k) - F(k-1) \approx 0$ (Cortes et al., 2009). Therefore, Equation 9 can be further simplified to

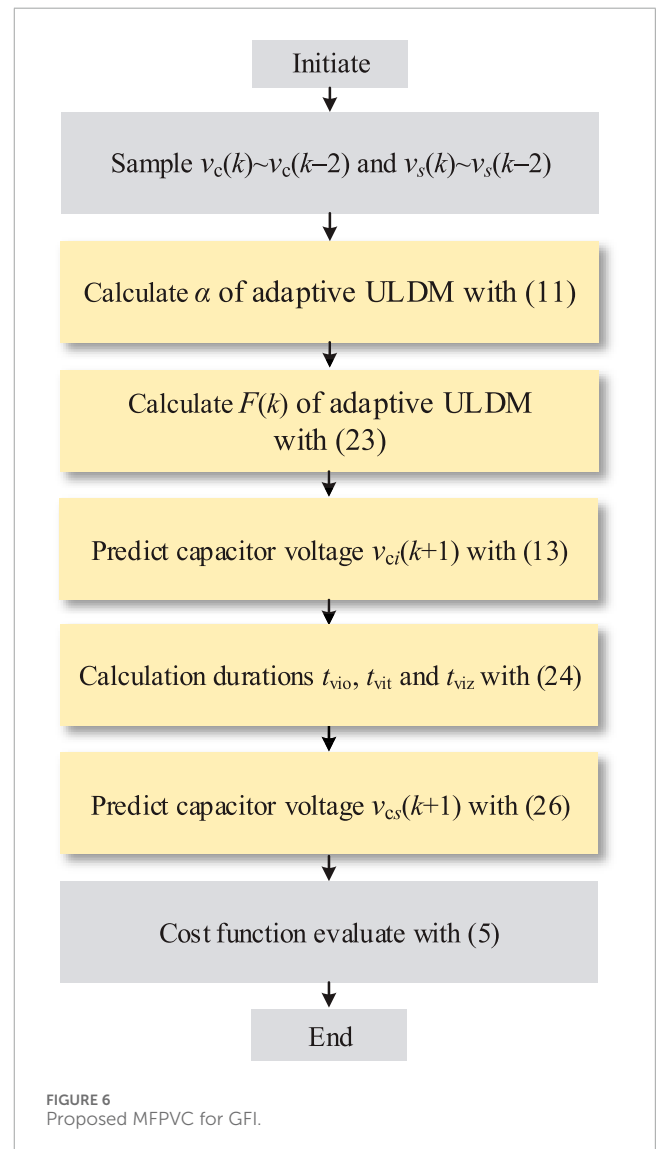$$g_c(k) - g_c(k-1) = \alpha\big(U_i(k-1) - U_i(k-2)\big).\qquad(10)$$

FIGURE 6
Proposed MFPVC for GFI.

Based on Equation 10, the gain of the ULDM can be expressed as

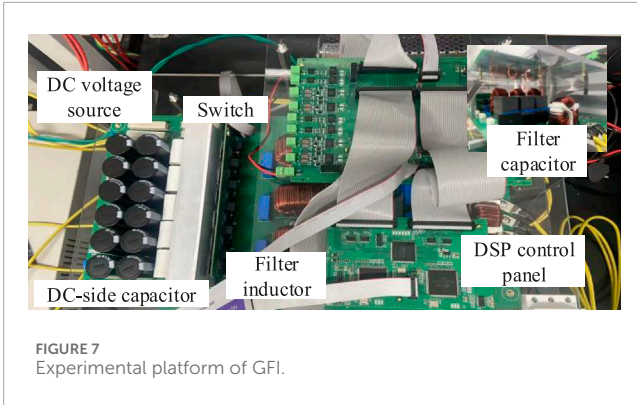$$\alpha = \frac{g_c(k) - g_c(k-1)}{U_i(k-1) - U_i(k-2)}.\qquad(11)$$

FIGURE 7
Experimental platform of GFI.

TABLE 2 Systems parameters.

Parameter	Value
DC voltage v_{dc}/V	200
Capacitor voltage reference v_{cref}/V	50, 80
Filter inductor L/mH	1.7
Filter capacitor C/μF	15
Load resistance R/Ω	10
Control period T_s/μs	50

Substituting Equation 11 into Equation 7, the concentrated disturbance F of the ULDM can be expressed as

$$F(k) = g_c(k) - \frac{g_c(k) - g_c(k-1)}{U_i(k-1) - U_i(k-2)} U_i(k-1). \quad (12)$$

Using α from Equation 11 and $F(k)$ from Equation 12, the model-free voltage prediction $v_{ci}(k+1)$ is obtained as

$$v_{ci}(k+1) = v_c(k) + T_s(\alpha U_i(k+1) + F(k))F(k) = g_c(k)$$
$$- \frac{g_c(k) - g_c(k-1)}{U_i(k-1) - U_i(k-2)} U_i(k-1). \quad (13)$$

It can be observed from Equation 13 that the capacitor voltage can be predicted based on the obtained gain and concentrated disturbance of the ULDM, which are obtained from the measuring voltage data, eliminating parametric effect on voltage prediction.

3.1.3 Design of adaptive ultra-local data-model

It should be noted that the calculation of α and F in the ULDM would have a larger error when the sampling frequency is low, leading to poor control effect of MFPC. To effectively estimate the α and F in the ULDM, the linear extended-state-observer (LESO) is designed to estimate the α and F in the ULDM. The system state equation in Equation 6 can be written as

$$\begin{cases} \dfrac{d\hat{v}_c}{dt} = \alpha U_i + \hat{F} + \delta_1(v_c - \hat{v}_c) \\ \dfrac{d\hat{F}}{dt} = \delta_2(v_c - \hat{v}_c) \end{cases}, \quad (14)$$

where δ_1 and δ_2 are the error gain of the voltage estimation and the concentrated disturbance estimation, respectively. The superscript $^$ represents the estimated value. Equation 14 can be discretized and expressed as

$$\begin{cases} \hat{v}_c(k+1) = \hat{v}_c(k) + T_s(\alpha U_i(k) + \hat{F}(k) + \delta_1(v_c(k) - \hat{v}_c(k))) \\ \hat{F}(k+1) = \hat{F}(k) + T_s\delta_2(v_c(k) - \hat{v}_c(k)) \end{cases}, \quad (15)$$

The matrix form of Equation 15 can be expressed as

$$\underbrace{\begin{bmatrix} \hat{v}_c(k+1) \\ \hat{F}(k+1) \end{bmatrix}}_{\hat{x}(k+1)} = \underbrace{\begin{bmatrix} 1 & T_s \\ 0 & 1 \end{bmatrix}}_{G} \underbrace{\begin{bmatrix} \hat{v}_c(k) \\ \hat{F}(k) \end{bmatrix}}_{\hat{x}(k)} + \underbrace{\begin{bmatrix} T_s\alpha \\ 0 \end{bmatrix}}_{H} U_i(k)$$
$$+ \underbrace{\begin{bmatrix} T_s\delta_1 & 0 \\ T_s\delta_2 & 0 \end{bmatrix}}_{K} (v_c(k) - \hat{v}_c(k)). \quad (16)$$

In order to ensure the stability of the LESO, the eigenvalue of Equation 16 should be set in the unit circle of the z-plane. The characteristic polynomial of Equation 16 can be expressed as

$$|zI - (G - K)| = z^2 + (T_s\delta_1 - 2)z + 1 + T_s^2\delta_2 - T_s\delta_1, \quad (17)$$

where I is the second-order identity matrix. To obtain better robustness, the characteristic polynomial can be set as

$$|zI - (G - K)| = (z + \omega_0)^2, \quad (18)$$

where ω_0 is the bandwidth of the LESO. By combining Equations 17, 18, error gains δ_1 and δ_2 can be obtained as

$$\begin{cases} \delta_1 = \dfrac{2\omega_0 + 2}{T_s} \\ \delta_2 = \left(\dfrac{\omega_0 + 1}{T_s}\right)^2 \end{cases}. \quad (19)$$

By substituting the error gains δ_1 and δ_2 in Equation 19 into Equation 15, the observation of concentrated disturbance $F(k+1)$ can be achieved. To respond to the nonlinear changes of the GFI, the adaptive strengthening factor is designed in the LESO. Equation 14 can be further expressed as

$$\begin{cases} \dfrac{d\hat{v}_c}{dt} = \alpha U_i + \hat{F} + \tau\delta_1(v_c - \hat{v}_c) \\ \dfrac{d\hat{F}}{dt} = \tau\delta_2(v_c - \hat{v}_c) \end{cases}, \quad (20)$$

where τ is the adaptive strengthening factor, which can be expressed as

$$\begin{cases} \tau(k) = \hat{\theta}_1(k)e(k-1) + \hat{\theta}_2(k)\tau(k-1) \\ e(k) = |v_c(k) - \hat{v}_c(k)| \end{cases}, \quad (21)$$

where θ_1 and θ_2 are the system parameter vectors, which can be estimated in real time using the least square method, as

$$\begin{cases} \hat{\theta}(k) = \hat{\theta}(k-1) + K(k)(e(k) - \varphi^T(k)\hat{\theta}(k-1)) \\ K(k) = \dfrac{P(k-1)\varphi(k)}{\lambda + \varphi^T(k)P(k-1)\varphi(k)} \\ P(k) = \dfrac{(I - K(k)\varphi^T(k))P(k-1)}{\lambda} \end{cases}, \quad (22)$$
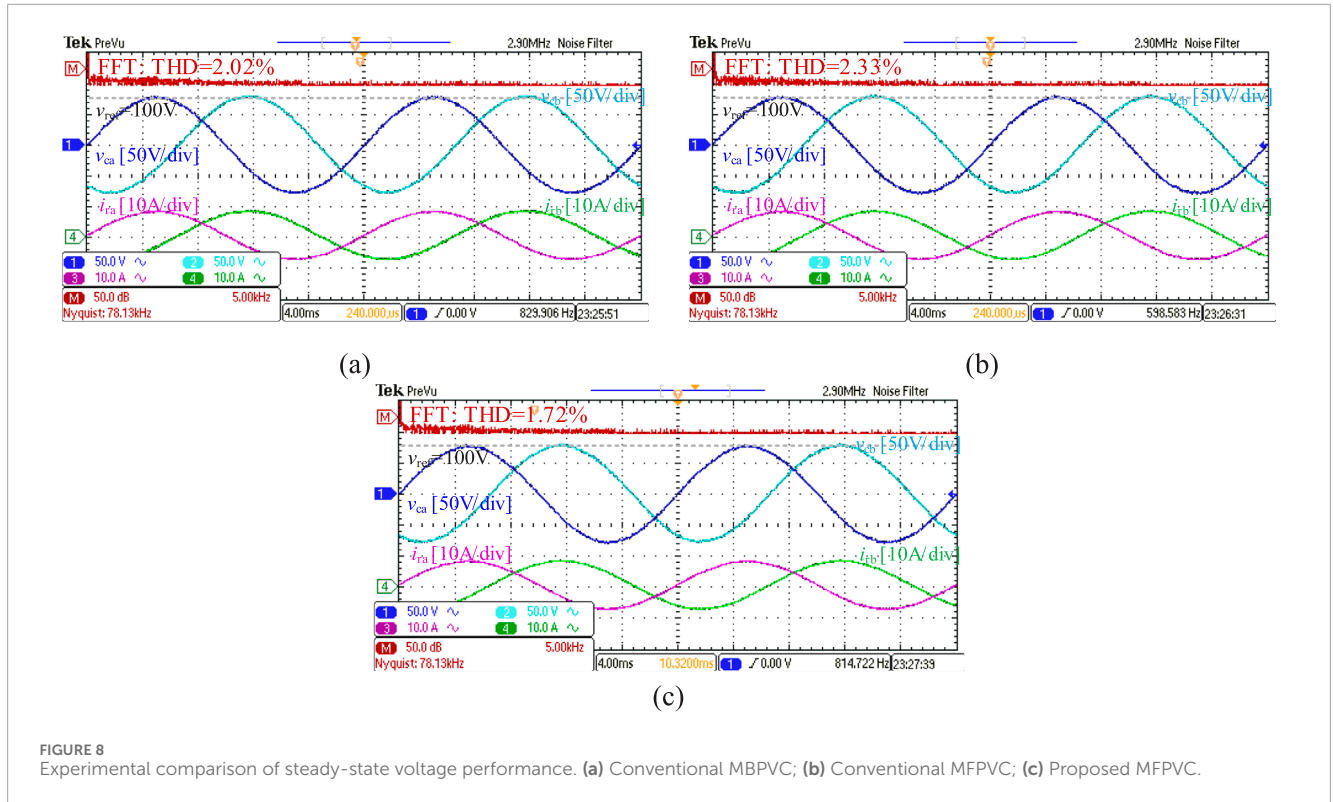
FIGURE 8
Experimental comparison of steady-state voltage performance. **(a)** Conventional MBPVC; **(b)** Conventional MFPVC; **(c)** Proposed MFPVC.

where $\varphi = [\tau \ e]^T$, $\theta = [\theta_1 \ \theta_2]^T$, λ is the forgetting factor, $\lambda \in [0.9, 1]$. K and P are the intermediate variables of the identification process, where the initial value of $P(0)$ can be set to 10^6. By combining the adaptive strengthening factor $\tau(k)$ in Figure 5 and the forward Euler method, Equation 20 can be discretized as

$$\begin{cases} \hat{v}_c(k+1) = \hat{v}_c(k) + T_s(\alpha U_i(k) + \hat{F}(k) + \delta_1 \tau(k)(v_c(k) - \hat{v}_c(k))) \\ \hat{F}(k+1) = \hat{F}(k) + T_s \delta_2 \tau(k)(v_c(k) - \hat{v}_c(k)) \end{cases} . \tag{23}$$

The ULDM relies on real-time estimation of the concentrated disturbance F and the gain α. The LESO dynamically adjusts these parameters by observing voltage tracking errors and updating $\hat{F}(k)$ through Equations 21–23. Specifically, the LESO feeds the estimated $\hat{F}(k)$ back into the ULDM Equation 13, enabling the model-free prediction to adapt to parameter variations and external disturbances. This closed-loop interaction ensures accurate voltage prediction even under parameter mismatches.

3.2 Proposed optimal switching sequence for GFI

3.2.1 Design of optimal switching sequence

To reduce the error of the proposed model-free voltage prediction, the basic voltage vector $v_i(k+1)$ in Equation 13 could be replaced with the combined voltage vector $v_{is}(k+1)$ ($s = 1, \ldots 6$), which is composed of two basic non-zero voltage vectors v_{i_o}, v_{i_t} ($v_1 \sim v_6$), and two zero voltage vectors v_{i_z} (v_0, v_7). The optimal

switching sequence of the combined voltage vector corresponding to each sector is summarized in Table 1. From Table 1, it can be observed that v_{i_o} is v_1, v_{i_t} is v_2, and v_{i_z} is v_0 and v_7 in section I. In other sections, v_{i_o} and v_{i_t} are replaced with others non-zero voltage vectors.

3.2.2 Design of optimal switching sequence

The durations t_{vio}, t_{vit} and t_{viz} corresponding to v_{i_o}, v_{i_t}, and v_{i_z}, respectively, can be obtained based on the deadbeat principle, as

$$\begin{cases} \partial g(t_{vio}, t_{vit})/\partial t_{vio} = 0 \\ \partial g(t_{vio}, t_{vit})/\partial t_{vit} = 0 \\ t_{viz} = T_s/4 - t_{vio}/2 - t_{vit}/2 \end{cases} . \tag{24}$$

Based on the durations t_{vio}, t_{vit} and t_{viz} from Equation 24 and the optimal switching sequence in Table 1, the model-free voltage prediction with optimal switching sequence can be obtained as

$$v_{cs}(k+1) = v_c(k) + 2t_{vio}(\alpha U_o(k+1) + F(k)) + 2t_{vit}(\alpha U_t(k+1) \\ + F(k)) + 4t_{viz}(\alpha U_z(k+1) + F(k)). \tag{25}$$

Based on Equations 7, 25 can be simplified as

$$v_{cs}(k+1) = v_c(k) + 2t_{vio}g_{co}(k+1) + 2t_{vit}g_{ct}(k+1) + 4t_{viz}g_{cz}(k+1). \tag{26}$$

Based on Equation 16, the model-free voltage prediction with optimal switching sequence can be obtained, which not only eliminate parametric effect, but also improve accuracy of voltage prediction, enabling the capacitor voltage performance in GFIs.
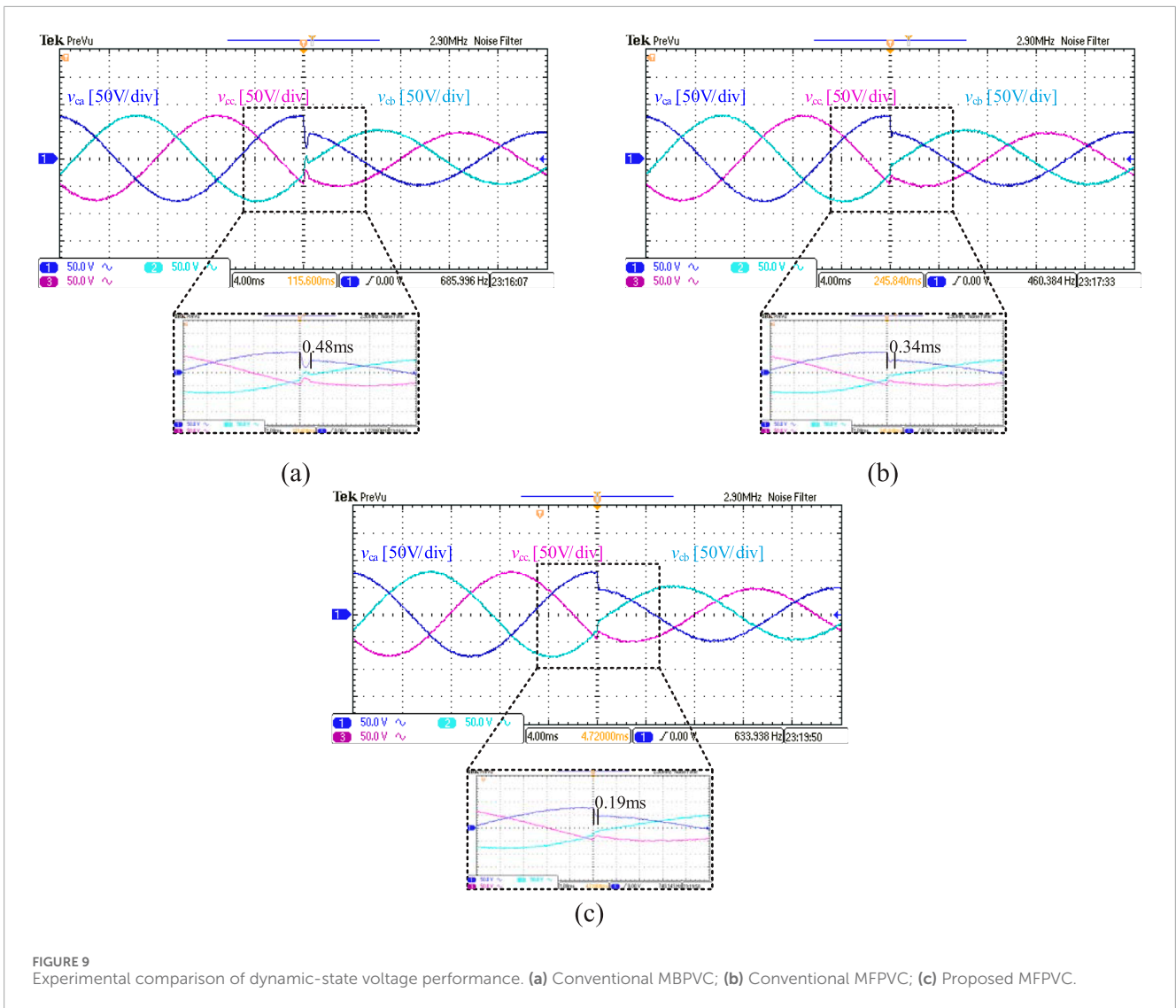
FIGURE 9
Experimental comparison of dynamic-state voltage performance. **(a)** Conventional MBPVC; **(b)** Conventional MFPVC; **(c)** Proposed MFPVC.

3.3 Proposed MFPVC strategy

Figure 6 illustrates the implementation flowchart of the proposed MFPVC strategy for GFIs. Initially, the capacitor voltage $v_c(k) \sim v_c(k-2)$ and voltage vector $v_{is}(k) \sim v_{is}(k-2)$ are sampled and substituted into Equations 11, 23 to calculate the gain α and the concentrated disturbance $F(k)$ of the ULDM, respectively. Subsequently, Equation 13 is used to predict the capacitor voltage $v_{ci}(k+1)$ corresponding to the basic voltage vector. By integrating the concept of deadbeat control and using Equation 24, the durations t_{vio}, t_{vit} and t_{viz} corresponding to the non-zero voltage vectors v_{i_o}, v_{i_t}, and two zero voltage vectors v_{i_z}, respectively, can be obtained. Based on the durations t_{vio}, t_{vit} and t_{viz}, the model-free voltage prediction with optimal switching sequence can be obtained with Equation 26, eliminating the influence of parameters on the voltage prediction. The combined voltage vector is substituted into Equation 5 to evaluate the prediction error corresponding to

each combined voltage vector. The combined voltage vector with smallest prediction error is selected as the optimal vector. The three-phase switch signals are applied based on Equation 1 in the next control period.

4 Experimental verification

To validate the effectiveness of the proposed MFPVC method, this section compares the grid-forming voltage performance of the conventional MBPVC method (Zheng et al., 2021), the conventional MFPVC method (Su et al., 2024), and the proposed MFPVC. The comparisons are conducted using the three-phase renewable energy grid-forming inverter experimental platform, as shown in Figure 7. The controller utilized is the TMS320C28335, and the experimental parameters are listed in Table 2.
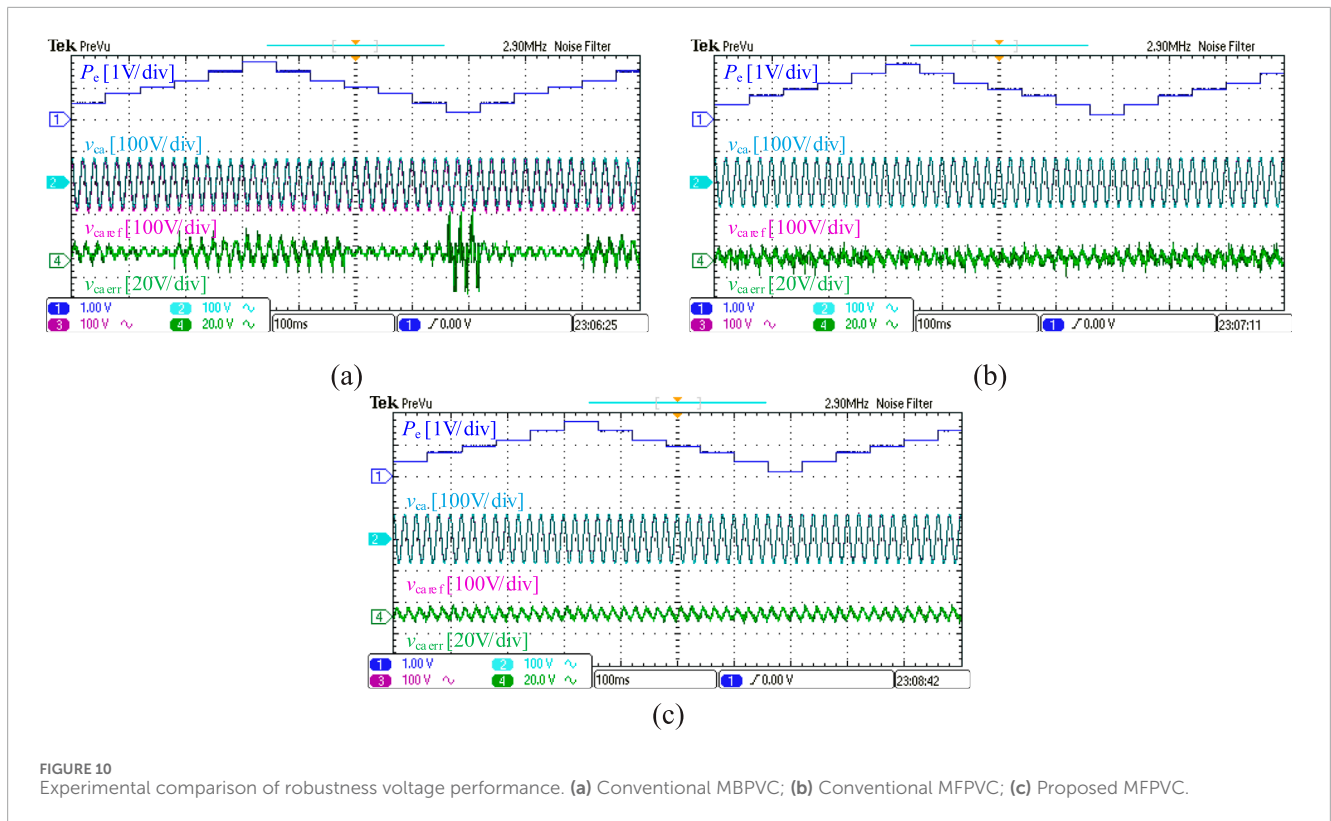
FIGURE 10
Experimental comparison of robustness voltage performance. **(a)** Conventional MBPVC; **(b)** Conventional MFPVC; **(c)** Proposed MFPVC.

TABLE 3 Voltage performance comparison.

Voltage performance	Methods		
	Conventional MBPVC	Conventional MFPVC	Proposed MFPVC
Steady-state voltage performance	THD = 2.02%	THD = 2.33%	THD = 1.72%
Dynamic-state voltage performance	0.48 ms	0.34 ms	0.19 ms
Robustness voltage performance	☆	☆☆	☆☆☆

Note: ☆ represents the worst performance; ☆☆ represents the medium performance; ☆☆☆ represents the optimal performance.

4.1 Experimental comparison of steady-state voltage performance

Figure 8 compares the steady-state voltage performance of the proposed MFPVC method, the conventional MBPVC method, and the conventional MFPVC method. The capacitor voltage reference v_{cref} is set at 80 V.

As shown in Figure 8a, when the conventional MBPVC method is applied, the steady-state voltage performance is good, with a Total Harmonic Distortion (THD) of 2.02%. In Figure 8b, the steady-state voltage performance reduces when the conventional MFPVC method is used, increasing the THD to 2.33%.

As illustrated in Figure 8c, the proposed MFPVC method achieves a voltage performance similar to that of the MBPVC method, with a THD of 1.72%, verifying the effectiveness of the proposed MFPVC method.

4.2 Experimental comparison of dynamic-state voltage performance

Figure 9 compares the dynamic-state voltage performance of the proposed MFPVC method, the conventional MBPVC method, and the conventional MFPVC method. The capacitor voltage reference v_{cref} is changed from 80 V to 50 V.

As shown in Figure 9a, when the conventional MBPVC method is applied, its dynamic-state voltage performance is relatively poor, with a response speed of 0.48 ms. In Figure 9b, the dynamic voltage performance improves when the conventional MFPVC method is used due to that the conventional MFPVC is applied based on the voltage and current difference, which is simpler than conventional mathematical model, reducing the response speed to 0.34 ms.

As illustrated in Figure 9c, the proposed MFPVC method achieves the best dynamic-state voltage performance due to the use

of adaptive ULMD, with a response speed of 0.19 ms, verifying the effectiveness of the proposed MFPVC method.

4.3 Experimental comparison of robustness voltage performance

Figure 10 compares the robustness voltage performance of the proposed MFPVC method, the conventional MBPVC method, and the conventional MFPVC method. The capacitor voltage reference v_{cref} is 80 V. The parameter error P_e is changed from 0.2 to 1.8.

As shown in Figure 10a, when the conventional MBPVC method is applied, its robustness voltage performance is obviously affected due to that the conventional MBPVC depends on the accurate parameter. When parameter errors P_e increase, the voltage errors also increase. In Figure 10b, the robustness voltage performance improves when the conventional MFPVC method is used due to the use of the voltage and current difference, which replaces the conventional mathematical model, improving the robustness. However, conventional MFPVC is easily affected by sampling noise, increasing voltage errors.

As illustrated in Figure 10c, the proposed MFPVC method achieves the best robustness voltage performance due to the use of ultra-local data-model, verifying the effectiveness of the proposed MFPVC.

4.4 Experimental comparison summary

As illustrated in Table 3, the proposed MFPVC with THD of 1.72% achieves comparable steady-state voltage performance to the conventional MBPVC with THD of 2.02% and superior voltage performance compared to the conventional MFPVC with THD of 2.33%. Besides, the dynamic performance of proposed MFPVC is 0.29 ms, which has the best dynamic-state voltage performance compared to conventional MBPVC method and conventional MFPVC method. Furthermore, proposed MFPVC demonstrates the best robustness compared to conventional MBPVC and conventional MFPVC under mismatched parameters.

5 Conclusion

This paper proposes an improved model-free predictive voltage control (MFPVC) for grid-forming inverters (GFIs) in renewable energy systems. The proposed MFPVC establishes and updates the adaptive ultra-local data-model (ULDM) for the GFI, eliminating the impact of parameters on voltage prediction. Additionally, to further reduce prediction errors, the proposed MFPVC designs an optimal switching sequence and calculates the duration using the deadbeat principle.

Various experiments are conducted to validate the effectiveness of the proposed MFPVC, showing: (1) When parameters are accurate, the proposed MFPVC with THD of 1.72% achieves comparable steady-state performance to the conventional MBPVC with THD of 2.02% and superior voltage performance compared

to the conventional MFPVC with THD of 2.33%; (2) The dynamic performance of the proposed method is 0.29 ms faster than that of the conventional MBPVC method and 0.15 ms faster than that of the conventional MFPVC method; (3) It demonstrates greater robustness compared to conventional MBPVC under mismatched parameters.

In the future, we can study the application of the proposed MFPVC in LCL filter grid-connected inverters and study the application of the proposed MFPVC in high-power and low-switching frequency GFIs, improving the application range of the proposed MFPVC in more complex micro-grid.

Data availability statement

The original contributions presented in the study are included in the article/supplementary material, further inquiries can be directed to the corresponding author.

Author contributions

YL: Conceptualization, Writing–original draft, Writing–review and editing. JZ: Funding acquisition, Writing–review and editing. FH: Investigation, Writing–review and editing.

Conflict of interest

Author YL was employed by Country State Grid Fujian Electric Power Co., Ltd. Authors JZ and FH were employed by Putian Electric Power Supply Company of State Grid Fujian Electric Power Co., Ltd.

Generative AI statement

The authors declare that no Generative AI was used in the creation of this manuscript.

Publisher's note

All claims expressed in this article are solely those of the authors and do not necessarily represent those of their affiliated organizations, or those of the publisher, the editors and the reviewers. Any product that may be evaluated in this article, or claim that may be made by its manufacturer, is not guaranteed or endorsed by the publisher.

References

Cortes, P., Ortiz, G., Yuz, J. I., Rodriguez, J., Vazquez, S., and Franquelo, L. G. (2009). Model predictive control of an inverter with output LC filter for UPS applications. *IEEE Trans. Industrial Electron.* 56 (6), 1875–1883. doi:10.1109/tie.2009.2015750

Heydari, R., Young, H., Bahamonde, F. F., Zadeh, S. V., Castano, C. G., Sabzevari, S., et al. (2022). Model-free predictive control of grid-forming inverters with LCL filters. *IEEE Trans. Power Electron.* 37 (8), 9200–9211. doi:10.1109/TPEL.2022.3159730

Hu, C., Xu, W., Yin, Z., Rui, T., Zhang, Z., Lu, G., et al. (2024). A novel modulated model-free predictive control for LC-filtered grid-forming inverters with double-difference updating. *IEEE Trans. Industrial Electron.* 71 (9), 10806–10817. doi:10.1109/tie.2023.3335463

Hu, C., Yin, Z., Rui, T., Zhang, Z., Shen, W., Cao, W., et al. (2023). A novel double-voltage-vector model-free predictive current control method for two-level voltage source inverters. *IEEE Trans. Industrial Electron.* 70 (6), 5872–5884. doi:10.1109/tie.2022.3199947

Jin, N., Chen, M., Guo, L., Li, Y., and Chen, Y. (2022). Double-vector model-free predictive control method for voltage source inverter with visualization analysis. *IEEE Trans. Industrial Electron.* 69 (10), 10066–10078. doi:10.1109/tie.2021.3128905

Lian, C., Xiao, F., Liu, J., and Gao, S. (2023). Parameter and VSI nonlinearity hybrid estimation for PMSM drives based on recursive least square. *IEEE Trans. Transp. Electrification* 9 (2), 2195–2206. doi:10.1109/tte.2022.3206606

Liu, T., and Wang, X. (2022). Physical insight into hybrid-synchronization-controlled grid-forming inverters under large disturbances. *IEEE Trans. Power Electron.* 37 (10), 11475–11480. doi:10.1109/tpel.2022.3168902

Long, B., Yang, W., Hu, Q., Guerrero, J. M., Carcia, C., Rodriguez, J., et al. (2022b). Moth–flame-optimization-based parameter estimation for FCS-MPC-Controlled grid-connected converter with LCL filter. *IEEE J. Emerg. Sel. Top. Power Electron.* 10 (4), 4102–4114. doi:10.1109/jestpe.2022.3140228

Long, B., Zhu, Z., Yang, W., Chong, K. T., Rodriguez, J., and Guerrero, J. M. (2022a). Gradient descent optimization based parameter identification for FCS-MPC Control of LCL-type grid connected converter. *IEEE Trans. Industrial Electron.* 69 (3), 2631–2643. doi:10.1109/tie.2021.3063867

Rui, T., Feng, Z., Hu, C., Yin, Z., Cao, W., Lu, G., et al. (2024). Double-vector model-free predictive current control method for voltage source inverters with sampling noise suppression. *IEEE Trans. Industrial Electron.* 71 (6), 5797–5806. doi:10.1109/tie.2023.3273241

Rui, T., Yin, Z., Hu, C., Lu, G., Zhang, P., Shen, W., et al. (2023). Modulated model-free predictive current control for voltage source inverters with stagnation elimination and sampling disturbance suppression. *IEEE Trans. Power Electron.* 38 (6), 6996–7008. doi:10.1109/tpel.2023.3247811

Samanta, S., Lagoa, C. M., and Chaudhuri, N. R. (2024). Nonlinear model predictive control for droop-based grid forming converters providing fast frequency support. *IEEE Trans. Power Deliv.* 39 (2), 790–800. doi:10.1109/tpwrd.2023.3336868

Song, G., Cao, B., and Chang, L. (2022). Review of grid-forming inverters in support of power system operation. *Chin. J. Electr. Eng.* 8 (1), 1–15. doi:10.23919/cjee.2022.000001

Su, G., Li, H., Li, Z., and Zhou, Y. (2024). Model-free control of permanent magnet synchronous linear motor based on ultra-local model. *Chin. J. Electr. Eng.* 10 (4), 73–82. doi:10.23919/CJEE.2024.000050

Tan, S., Xie, P., Guerrero, J. M., Vasquez, J. C., Alcala, J. M., Carreno, J. E. M., et al. (2024). Lyapunov-based resilient cooperative control for DC microgrid clusters against false data injection cyber-attacks. *IEEE Trans. Smart Grid* 15 (3), 3208–3222. doi:10.1109/tsg.2023.3332946

Yin, Z., Deng, F., Ghanem, A., Kaddah, S. S., and Abulanwar, S. (2024b). PLPR-based predictive control for LCL-filtered voltage source inverters. *IEEE Trans. Power Electron.* 39 (6), 7468–7480. doi:10.1109/tpel.2024.3371053

Yin, Z., Deng, F., Kaddah, S. S., and Abulanwar, S. (2024a). Modulated PLPR-based predictive control with noise suppression for LC-filtered voltage source inverters. *IEEE Trans. Industrial Electron.* 72 (3), 2588–2598. doi:10.1109/tie.2024.3433438

Zhang, Y., Jin, J., and Huang, L. (2021). Model-free predictive current control of PMSM drives based on extended state observer using ultralocal model. *IEEE Trans. Industrial Electron.* 68 (2), 993–1003. doi:10.1109/tie.2020.2970660

Zhao, T., Zhang, M., Wang, C., and Sun, Q. (2023). Model-free predictive current control of three-level grid-connected inverters with LCL filters based on kalman filter. *IEEE Access* 11, 21631–21640. doi:10.1109/access.2023.3251410

Zheng, C., Dragičević, T., Zhang, Z., Rodriguez, J., and Blaabjerg, F. (2021). Model predictive control of LC-filtered voltage source inverters with optimal switching sequence. *IEEE Trans. Power Electron.* 36 (3), 3422–3436. doi:10.1109/tpel.2020.3015540